NJC

New Journal of Chemistry

A journal for new directions in chemistry

Accepted Manuscript

This article can be cited before page numbers have been issued, to do this please use: S. S. Harmalkar, S. N. Dhuri, V. R. Chari and R. K. Kunkalekar, *New J. Chem.*, 2022, DOI: 10.1039/D2NJ04859K.

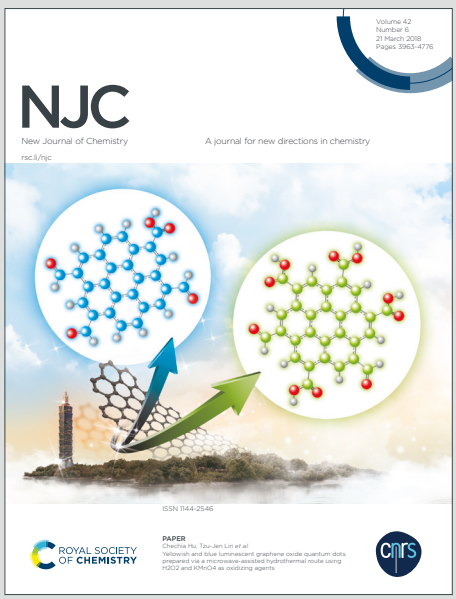

This is an Accepted Manuscript, which has been through the Royal Society of Chemistry peer review process and has been accepted for publication.

Accepted Manuscripts are published online shortly after acceptance, before technical editing, formatting and proof reading. Using this free service, authors can make their results available to the community, in citable form, before we publish the edited article. We will replace this Accepted Manuscript with the edited and formatted Advance Article as soon as it is available.

You can find more information about Accepted Manuscripts in the Information for Authors.

Please note that technical editing may introduce minor changes to the text and/or graphics, which may alter content. The journal's standard Terms & Conditions and the Ethical guidelines still apply. In no event shall the Royal Society of Chemistry be held responsible for any errors or omissions in this Accepted Manuscript or any consequences arising from the use of any information it contains.

View Article Online
DOI: 10.1039/D2NJ04859K

ARTICLE

Structure-function correlation of mononuclear nonheme copper(II) compounds based on ligand backbone effect and phenoxazinone synthase activity

Received 00th January 20xx,
Accepted 00th January 20xx

DOI: 10.1039/x0xx00000x

Sarvesh S. Harmalkar[a], Vishnu R. Chari[a], Rohan K. Kunkalekar[a], S. N. Dhuri[a]*

Mononuclear nonheme copper(II) compounds, $[Cu(BQEN)(CH_3CN)]^{2+}$ **1** and $[Cu(BQPN)(CH_3CN)]^{2+}$ **2** (BQEN = *N,N′*-dimethyl-*N,N′*-di(quinolin-8-yl)ethaneane-1,2-diamine; BQPN = *N,N′*-dimethyl-*N,N′*-di(quinolin-8-yl)propane-1,2-diamine) are synthesised and characterized by elemental analysis, ESI-MS, EPR and single crystal X-ray diffratrometry. Compound **1** crystalises in $P\bar{1}$ space group while **2** crystallises in $P2_1/n$. Compounds **1** and **2** exhibit distorted square pyramidal geometry which deviate interestingly by 4.8 and 48.0 % from a regular square pyramidal structure in **1** and **2** respectively. This is attributed to the marginal increase in the carbon chain backbone of ligand in **2**. Compounds **1** and **2** have been used in aerial oxidation of 2-aminophenol (H_2AP) to 2-amino-phenoxazine-3-one (APX) which revealed phenoxazinone synthase activity. The DFT steric maps were utilized to understand the catalytic activity of **1** (%Vbur, 71.3 %) and **2** (%Vbur, 75.6 %). The current results clearly demonstrate an interesting structure-function relationship based on the effect of ligand backbone on the geometry.

Introduction

Enzymes are the most enthralling macromolecular molecules in nature with versatile structure. Metalloenzymes which are a significant group of enzymes have a metal core in their active site usually a transition metal core owing to their unique characteristic properties such as variable oxidation states [1]. The recent developments in bioinorganic chemistry have witnessed many attempts to mimic these metalloenzymes that brings better understanding of their properties connected with various.

The model inorganic compounds are composed of the metal core and a suitable ligand as a stabilizer to metal ion. The bioinorganic chemists have designed and studied a large number of transition metal compounds by tuning the carbon backbone and donor atoms of coordinating ligands. This has resulted in understanding of the rich diversity and versatility in their structural and functional properties. The tunability of the ligands have played major role in perturbing intrinsic properties which directly affects the rate of reaction, selectivity of the substrate binding and product formation and yields, the stability and traceability of intermediates and the enzymatic activity. In recent times we have been successful in designing several nonheme ligand skeletons and practically metallated all of them to from stable compounds with rich applications and reactivities. In the quest of doing this, a selection of an appropriate metal ion that can embrace all complexities of ligands is a vital factor. The coinage metal namely copper in third row of transition metals is well known for its flexibility to adopt various coordination geometries based on the steric constraints manifested by the ligands. For instance, the penta-coordinated Cu(II) compounds adopts square pyramidal (sp), trigonal bipyramidal (tbp) geometries or a geometry in between the two these extremes. For the first time Addison and co-workers in 1984 introduced the trigonality parameter ($\tau 5$) to understand the cause of deviation from the ideal geometries [2]. After two decades, Houser and co-workers introduced another geometric parameter ($\tau 4$) for the four-coordinated transition metal compounds [3]. One way to study the gradual change in geometrical features of the metal compounds is by adopting mixed ligands based on their steric factors. The Cu(II) compounds of mixed ligands have captivated the attention of many researchers not only owing to their fascinating structures which influence their photophysical properties [4], but also due to their

[a] *School of Chemical Sciences, Goa University, Goa-403206, India. sndhuri@unigoa.ac.in*

† CCDC Numbers 2095957 and 2095956 contain the supplementary crystallographic data of compounds 1 and **2**. This data can be obtained free of charge via www.ccdc.cam.ac.uk/data_request/cif or data_request@ccdc.cam.ac.uk or by contacting The Cambridge Crystallographic Data Centre, 12 Union Road, Cambridge CB2 1EZ, U.K.; fax: +44 1223 336033.

Electronic Supplementary Information (ESI) available: [details of any supplementary information available should be included here]. See DOI: 10.1039/x0xx00000x

View Article Online
DOI: 10.1039/D2NJ04859K

exceptional anticancer activity which has a potential to replace the expensive platinum metal based drugs [5].

Another aspect of selecting copper is its high abundance in different biological metalloenzymes in Cu(II) & Cu(I) ion forms. The metalloenzymes containing copper at active site have been known to play vital roles in dioxygen transportation [6], quercetin 2,3-dioxygenase [7-9] and catechol oxidase reaction [10], catalytic oxidation of aromatic rings in tyrosine [11], methane oxidation as methane monoxygenase [12-14] as well as in hydrogen peroxide formation in glyoxal and galactose oxidase [15-18].

Another oxygen activating copper containing metalloenzyme is phenoxazinone synthase (PHS) [19-23]. PHS is a type of multicopper oxidase enzyme which catalyses dimerization of 2-aminophenol (H_2AP) in the presence of dioxygen to 2-aminophenoxazinone species (APX). This bioinspired oxidation is the crucial final step for the biosynthesis of actinomycin D which is a powerful antineoplastic agent [24-27] used in clinical treatment of gestational choriocarcinoma, Wilm's tumour and other tumour cells [23]. Begley and co-workers demonstrated that the oxidative dimerization reaction involves three two-electron transfer steps leading to a six-electron oxidation [20]. PHS was structurally characterised and known exhibit dimeric and hexameric oligomeric forms [22].

The various bioinspired models have been studied owing to availability of a literature on structural and functional properties of PHS [23, 28-35]. A tetranuclear cubane-like Cu(II) core was first reported by Chaudhuri and co-workers which could catalyse the oxidation of H_2AP to APX in the presence of molecular oxygen [28]. Few more tetranuclear centres were later reported as the possible mimics of PHS [29]. Apart from the cubane centres, the several heterometallic Cu-Mn compounds have been studied as PHS models [30]. The dimeric Cu(II) compounds have been reported and found to be very effective in the aerobic conversion of H_2AP to APX [31]. In addition, a several mononuclear compounds are reported to mimic PHS property. In this respect not only Cu [32] but other metals like Mn [33], Fe [34], Co [35] have been used to prepare mononuclear mimic of PHS.

Although many reports on PHS mimics exists, there is a need to obtain more clarity on the understanding of structure-function relationship, dioxygen activation pathways, mechanistic aspects and several other factors involved in the PHS activity. Hence, there is ample scope to investigate and explore this area in the current time.

In our continuous efforts to understand structure-reactivity correlations and patterns, herein we have investigated phenoxazinone synthase (PHS)-like activity of two novel new Cu(II) compounds viz. $[Cu(BQEN)(CH_3CN)](ClO_4)_2$ **1** and $[Cu(BQPN)(CH_3CN)](ClO_4)_2$ **2** bearing nonheme tetradentate N4 ligands, (BQEN = N,N'-dimethyl-N,N'-di(quinolin-8-yl)ethaneane-1,2-diamine and BQPN = N,N'-dimethyl-N,N'-di(quinolin-8-yl)propane-1,2-diamine). BQEN and BQPN (Fig. 1) differ only in their carbon chain backbones by one carbon that has led to form two different geometries for **1** and **2** (*vide infra*). In our earlier work [36], we have synthesised Ni(II) compounds of containing BQEN and demonstrated the *cis*-ligand substitution effect on the reactivity of alkanes to alcohols.

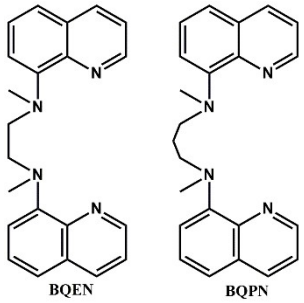

Fig. 1. Chemical structures of ligands; BQEN and BQPN used in this study.

Experimental

Material and methods

All chemicals used in this work were of analytical grade and used without any further purification. The ligands namely BQEN and BQEPN were synthesised by following the reported procedures [36]. Infra-red (IR) spectra were recorded using Shimadzu (IR-Prestige-21) FT-IR spectrometer in the region from 4000–400 cm^{-1}. UV-visible spectra were measured on Agilent UV-Visible spectrophotometer (8453 model) using standard and kinetic modes. Elemental analyses (C,H,N) were performed on Elementar Variomicro Cube CHNS Analyser. The single crystal X-ray structures of **1** and **2** were determined using Bruker D8 Quest Eco X-ray diffractometer. Intensity data were collected at room temperature (RT) using monochromated (MoKα = 0.7107 Å) radiation. The program suite APEX3 (Version 2018.1) was used to integrate the frames, to perform absorption correction and to determine unit cell. The structures were solved with SHELXS and subsequent refinements were performed with SHELXL [37]. The structure refinement parameters of **1** and **2** are given in Table S1. The organic products formed in the reactions

View Article Online
DOI: 10.1039/D2NJ04859K

were analysed using the Shimadzu GC 2014 equipped with HP capillary column (30 m × 0.25 mm × 2.5 μM) and an FID detector. The retention time and peak areas of the products were compared with authentic samples using decane as an internal standard. The X-band EPR measurements were performed at 77 K on a JEOL X-band spectrometer (JESFA100). The *g* value was calibrated using the manganese marker. The geometry optimizations were performed using density functional theory (DFT). For geometry optimization the asymmetric unit shown in Fig. 2a (for **1**) and Fig. 3a (for **2**) is considered. These calculations were performed at B3LYP/6-31++G(d, p) level of theory in gas phase using Gaussian 16 program suite [38]. The frequency calculation at the same level of theory were performed to confirm that the optimized structure is a minimum on the potential energy surface. The steric maps were obtained using a web application, SambVca 2.1 available at https://www.molnac.unisa.it/Omtools/sambvca2.1/index.html [39]. The optimized geometry structures were used for the calculations of steric maps.

Results and discussion

Characterisation of compounds 1 and 2

The single crystals of **1** and **2** were grown by slow diffusion method in which diethylether was added slowly to the acetonitrile solution of compounds **1** and **2**. Compound **1** crystallises in triclinic space group *P*$\bar{1}$ while **2** crystallises in a monoclinic $P2_1/n$ space group. The technical details of data collection and selected refinement parameters for **1** and **2** are given in Table 1. The crystal structure of **1** contains Cu(II) cation, a BQEN molecule functioning as tetradentate ligand and a coordinated acetonitrile molecule leading to a penta-coordinate distorted square pyramidal (SP) geometry around the copper(II) (Fig. 2a). The distances of copper(II) from the quinoline nitrogens N1 and N4 are 2.004(2) and 1.973(2) Å respectively while amine nitrogens N2 and N3 are away from copper(II) by 2.275(3) and 2.126(2) Å respectively. The Cu(II) ion is coordinated to N of CH_3CN by a distance of 2.036(3) Å (Table S1). The axial positions of SP geometry are occupied by N2 while the equatorial positions are occupied by N1, N3, N4 and N5. The bond angles N1-Cu-N3; 94.62, N3-Cu-N4; 83.28, N4-Cu-N5; 92.84 and N1-Cu-N5; 89.11 sums to 359.85˚, the value which is very close to the expected 360˚ indicating that the structure of **1** is slightly distorted. The structure of **1** is completed by perchlorate ions which act as the counter anions and are involved in weak hydrogen bonding interactions with the cations (Table S2 and Fig. 2b). The cations form dimeric units through the C-H···H-C interactions with a distance of 2.371 Å (Fig. S2).

Crystal structure of **2** contains Cu(II) cation, a BQPN tetradentate ligand and a coordinated acetonitrile molecule leading to a penta-coordinate geometry (Fig. 3a). The difference in BQEN and BQPN is the only presence of addition carbon backbone in terms of -CH_2- group. The distances of copper from the quinoline nitrogens N1 and N4 are 1.994(3) and 2.024(2) Å respectively while the amine nitrogens N2 and N3 are separated from copper(II) by distance of 2.096(2) and 2.053(3) Å respectively. On the other hand the Cu(II) ion is away from N atom of CH_3CN by distance of 2.283(3) Å (Table S3). The axial positions of SP geometry are occupied by N5 atom while the equatorial positions are occupied by N1, N2, N3 and N4 donor atoms. The bond angles N1-Cu-N2; 81.99, N2-Cu-N3; 96.16, N3-Cu-N4; 84.03 and N1-Cu-N4; 98.90 sums to 361.08˚, the value which is close to the expected 360˚ but higher the value observed in **1** indicating slightly more distortion of SP geometry in **2**. Like in **1**, the perchlorate counter anions are involved in hydrogen bonding interactions with the cations (Table S4 and Fig. 3b). The cation forms one-dimensional chain along the *b* axis curtsey of the π···π interactions with a distance of 3.412 Å (Fig. S4).

Table 1 - Crystal data and structure refinement of **1** and **2**.

Compound	**1**	**2**
Empirical formula	$C_{24}H_{25}Cl_2CuN_5O_8$	$C_{25}H_{27}Cl_2CuN_5O_8$
Formula weight	645.94	659.97
Temperature	296(2) K	296(2) K
Wavelength	0.71073 Å	0.71073 Å
Crystal system	Triclinic	Monoclinic
Space group	*P*-1	$P2_1/n$
Unit cell dimensions	a = 8.8978(2) Å b = 12.9429(3) Å c = 13.0536(3) Å α = 89.5050(10)° β = 71.2600(10)° γ = 74.5360(10)°	a = 8.6168(3) Å b = 19.1651(7) Å c = 16.7109(7) Å α = 90° β = 93.2210(10)° γ = 90°
Volume	1367.17(6) $Å^3$	2755.31(18) $Å^3$
Z	2	4
Density (calculated)	1.569 Mg/m^3	1.591 Mg/m^3
Absorption coefficient	1.051 mm^{-1}	1.045 mm^{-1}
F(000)	662	1356
Crystal size	0.45 x 0.32 x 0.21 mm^3	0.55 x 0.33 x 0.11 mm^3
Theta range for data collection	2.593 to 28.282°.	2.595 to 26.387°.
Index ranges	-11<=h<=11, -17<=k<=17, -17<=l<=17	-10<=h<=10, -23<=k<=23, -20<=l<=20
Reflections collected	32636	33466

View Article Online DOI: 10.1039/D2NJ04859K

Independent reflections	7922 [R(int) = 0.0380]	5615 [R(int) = 0.0344]
Completeness to theta = 25.242°	99.9 %	99.8 %
Absorption correction	Semi-empirical from equivalents	Semi-empirical from equivalents
Refinement method	Full-matrix least-squares on F^2	Full-matrix least-squares on F^2
Data / restraints / parameters	6769 / 0 / 364	5615 / 0 / 373
Goodness-of-fit on F^2	1.035	1.057
Final R indices [I>2sigma(I)]	R1 = 0.0517, wR2 = 0.1479	R1 = 0.0469, wR2 = 0.1311
R indices (all data)	R1 = 0.0651, wR2 = 0.1617	R1 = 0.0611, wR2 = 0.1450
Extinction coefficient	n/a	n/a
Largest diff. peak and hole	1.134 and -0.783 e.Å^{-3}	0.703 and -0.418 e.Å^{-3}

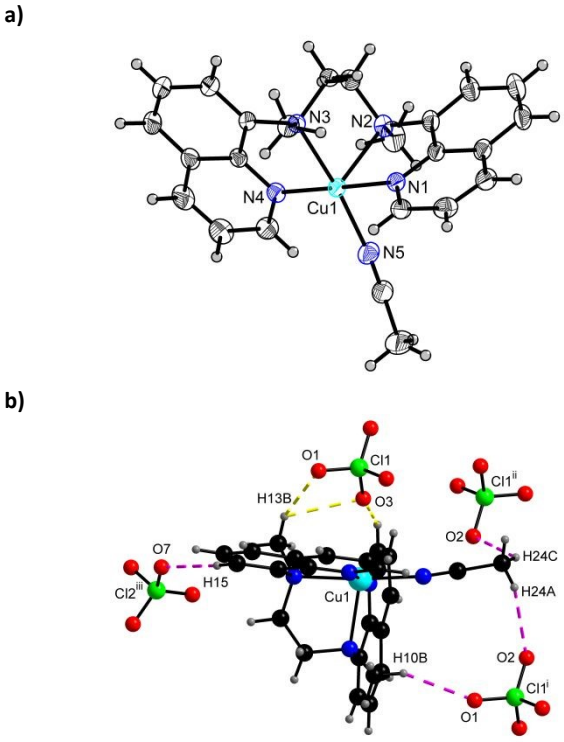

Fig. 2. (a) Crystal structure showing the asymmetric unit of **1**. (b) H-bonding situation around **1**. Symmetry codes: [i = x+1, y, z, ii = -x, -y+1, -z+1, iii = -x+1, -y+1, -z].

It is noted that both **1** and **2** exhibit distorted square pyramidal geometry while the only difference in **1** and **2** is the C chain length extended by one carbon in **2** (Fig. 1). The degree of distortion is known by τ (distortion index) given by the equation $\tau = \beta - \alpha / 60$ where α and β are the *trans* angles of the square base and the larger angle is considered as β. Typically defined as $\tau = 0$ for square pyramidal geometry and $\tau = 1$ for trigonal bipyramidal geometry [2]. Our results showed that **1** has τ value 0.048 (4.8 %) which is very close to the perfect square pyramidal geometry, while **2** has τ value of 0.46 (46.0 %) which suggest that **2** has a geometry intermediate between square pyramidal (SP) and trigonal bipyramidal (TBP). Thus addition of one carbon in the ligand backbone has emerged into a noticeable influence on the geometry and structure parameters of the compound **2**. Interestingly the level of distortion in **2** is quite high as compared to the other reported compounds of copper(II) stabilised by tetradendate N-donor ligands (Scheme 1 and Table 2) [40].

Compound **1** and **2** were characterized by EPR spectroscopy. The EPR spectrum of **1** is exhibited in Fig. S6. It can be clearly seen that there are two *g* values $g_{//}$ and $g_{\perp}$ which is typically seen for copper(II) compounds with square pyramidal geometry with $d_{x^2-y^2}$ as its ground state and a axial spectrum with equivalent x and y axes and two ***g*** values, $g_{//}$ (*gz*) and $g_{\perp}$ (*gx* = *gy*) [41].

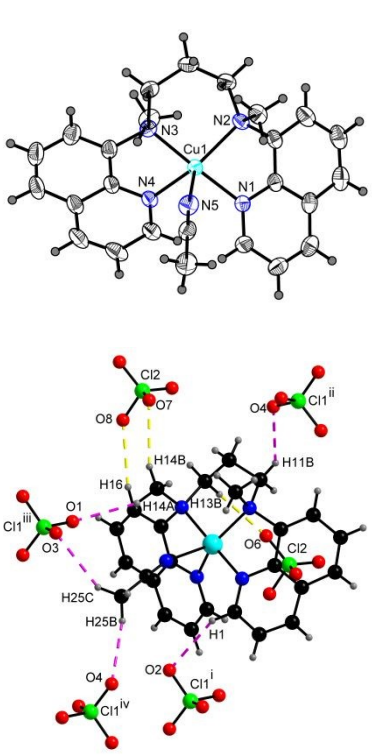

Fig. 3. (a) Crystal structure showing the asymmetric unit of **2**. (b) H-bonding situation around **2**. Symmetry codes: [i = -x+1/2, y-1/2, -z+1/2, ii = x+1, y, z, iii = -x+3/2, y-1/2, -z+1/2, iv = x+1/2, -y+3/2, z-1/2].

View Article Online
DOI: 10.1039/D2NJ04859K

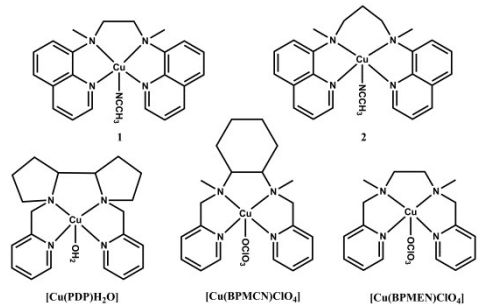

Scheme 1. Chemical structures of **1** and **2** along with report copper(II) compounds stabilized by tetradentate N-donor ligands

Table 2 – Comparison of structural parameter (τ) for **1** and **2** with known copper(II) compounds containing N-donor ligands

Compound	τ (distortion index)	Reference
1	0.04	*This work*
2	0.48	*This work*
$[Cu(PDP)H_2O]$	0.17	40a
$[Cu(BPMEN)ClO_4]$	0.36	40b
$[Cu(BPMCN)ClO_4]$	0.02	40c

The EPR spectrum of **2** is depicted in Fig. 4. The spectrum of **2** showed three *g* values g_x, g_y and g_z which are typically seen for other reported copper(II) compounds with geometry intermediate between square pyramidal and trigonal bipyramidal geometry with a linear combination of the $d_x^2-_y^2$ and d_z^2 orbitals as the ground state and a rhombic spectrum with $g_x > g_y > g_z$ [41]. These results from EPR data are consistent with the single crystal structure data (*vide supra*).

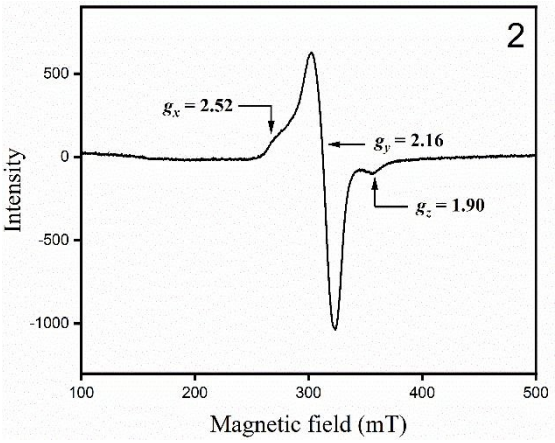

Fig. 4. X-band EPR spectra of **2** recorded at 77 K in CH_3CN.

Both compounds **1** and **2** were freely soluble in acetonitrile and we were able to measure their ESI-MS spectra. ESI-MS of **1** showed peaks at *m/z* 202.58, 222.58, 431.16 and 504.08, corresponding to $[Cu(BQEN)]^{2+}$ (calcd *m/z* 202.58), $[Cu(BQEN)(CH_3CN)]^{2+}$ (calcd *m/z* 223.07), $[Cu(BQEN)(CN)]^{1+}$ (calcd *m/z* 431.12) and $[Cu(BQEN)(ClO_4)]^{1+}$ (calcd *m/z* 504.06) (Fig. S7). While the ESI-MS of **2** (Fig 5) showed a prominent peak at 445.08 which corresponds to $[Cu(BQPN)(CN)]^{1+}$ (calcd *m/z* 445.13) [42].

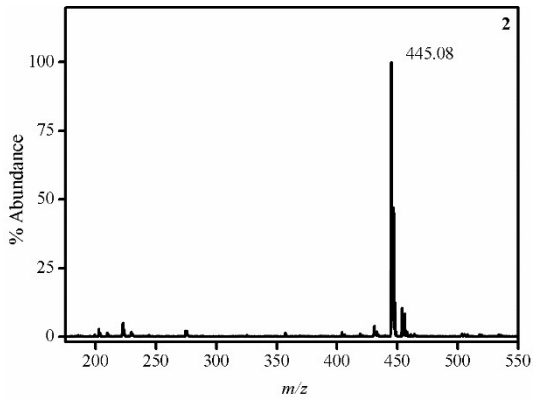

Fig. 5. ESI-MS spectrum of **2** recorded in CH_3CN.

Solid state IR spectra of **1** and **2** were recorded to infer the bands due to organic ligands BQEN and BQPN. The IR spectra both **1** and **2** are shown in Fig. S8. Both compounds shows bands corresponding to C-C, C-N, C-H similar to parent ligand molecules and are shifted slightly to lower wavenumbers indicating coordination with copper(II) ion to ligands. The weakly coordinated perchlorate anions in **1** and **2** showed well resolved absorption bands at 1093 (s) and 621 (m) cm^{-1} [43]. In order to understand the electronic structure of 1 and 2, compounds were studied by UV-visible spectroscopy using CH_3CN solvent. UV-visible spectra of **1** and **2** are shown in Fig. S9. The bands in the higher energy region are assigned due to intra-ligand charge transfer transitions viz n-π* (270-320 nm) and π-π*(220-230 nm) [44]. At higher concentrations, the compound **1** showed a band at 620 nm while **2** exhibited a band at 590 nm which are attributed to typical *d-d* transitions of copper(II) ion. The bands in the region of 580-660 nm range are shown by compounds having square pyramidal or distorted square pyramidal geometry and these are assigned to dxz, dxy → dz^2 transitions [45].

View Article Online
DOI: 10.1039/D2NJ04859K

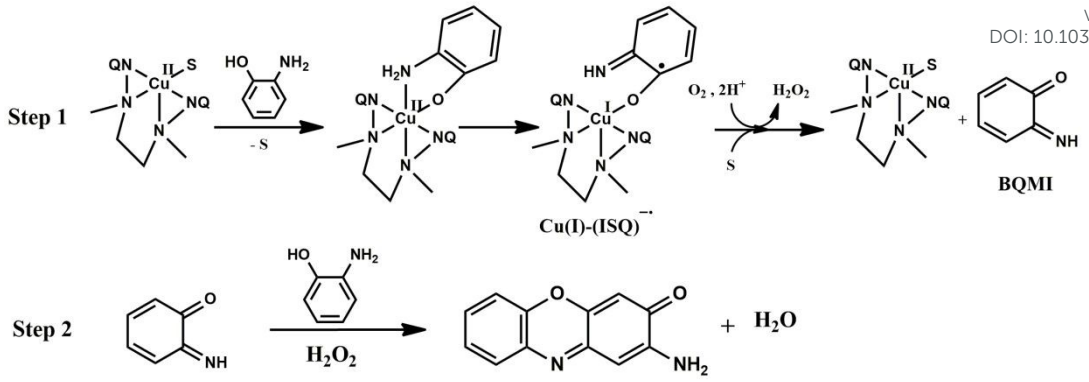

Scheme 2. Plusiable mechanism for the catalytic reaction

Phenoxazinone synthase activity and kinetic studies

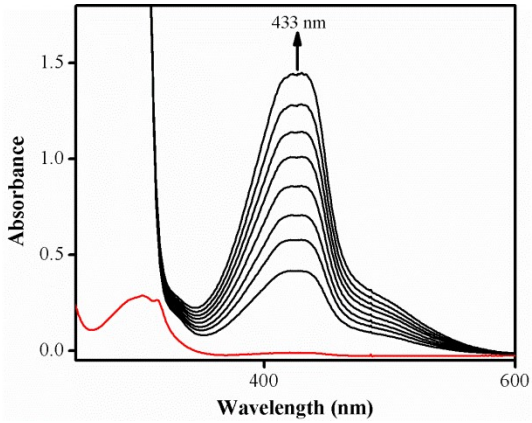

Fig. 6. UV-visible Spectral changes occurring at band at 433 nm on addition of 100 equivalents of substrate H_2AP to the methanolic solution of **1** due to the formation of aminophenoxazinone.

Since compounds 1 and 2 were structurally deviating from regular SP geometries, 1 being closer to regular SP geometry while 2 exhibiting pronounced distortion, we decided to investigate the reactivity of compounds **1** and **2** with 2-aminophenol (H2AP) which a model substrate for the phenoxazinone synthase activity. Compounds **1** and **2** were reacted H_2AP substrate in air saturated methanol solvent at room temperature (25 ℃). The reactions were carried out using 1 × 10^{-5} M concentrations of **1** and **2** and 1 × 10^{-3} M (100 equiv.) of H_2AP. The course of the reaction was followed by measuring the increase in absorbance at 433 nm band corresponding 2-aminophenoxazinone (APX) [47] as shown in (Fig. 6). The APX product formed was purified using column chromatography and characterised by NMR spectroscopy. H^1 NMR ($CDCl_3$, 400 MHz,) δ_H: 7.62 (m, 1H), 7.48 (m, 3H), 6.41 (s, 1H), 6.30 (s, 1H).

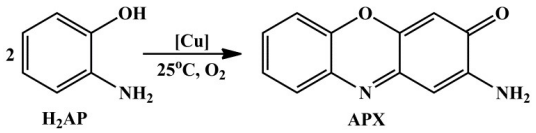

Scheme 3. Oxidation of H_2AP to phenoxazinone chromophore.

The catalytic reactions were carried out on a larger scale and the products formed were quantified by gas chromatography using decane as an internal standard and APX as standard sample. Product yields of 84 % and 72 % were obtained for compounds **1** and **2** respectively (Table 3). The TON of product formed in the reaction of **1** was higher compared to that observed in compound **2** (Table 3). Turnover number (TON) of the compounds were calculated by diving the number of moles of substrate converted by the mole of catalyst used.

Table 4 - Catalytic conversion of H_2AP [a]

Compound	Yield (%)	TON[b]
1	84	41.5
2	70	32.5

[a] Reaction conditions: catalyst = 1 × 10^{-5} mol, H_2AP = 1×10^{-3} mol (100 eq), temperature = 25℃, methanol = 5 mL.
[b] TON: number of moles of substrate converted per mole of catalyst.

Catalytic efficiency of the compounds was evaluated through a detailed kinetic study. The studies were carried out by taking a fixed amount of catalyst (1x10^{-6} M). The concentration of H_2AP was chosen such that it follows pseudo first order kinetics. The experiment was performed during a time span of 10 minutes for a particular set of compound-substrate mixture at maximum band of APX. All the reactions were carried out at temperature 25 ℃. The plots of initial rates (v_o versus concentration of substrate [H_2AP] show saturation behaviour for both the compounds as

seen in Fig. 7. The saturation kinetics indicate an intermediate compound-substrate adduct formation. The data was analysed using Michaelis-Menten hyperbolic equation 1 which is typically used in modelling enzymatic saturation kinetics [48].

$$\upsilon_o = \frac{V_{max}\,[H_2AP]}{K_M + [H_2AP]} \quad \text{eq. (1)}$$

The values of maximum rate of reaction (V_{max}) and Michaelis binding constant (K_M) were determined by a non-linear fit computer program (Origin 8.5) using equation (1). The catalytic turnovers (k_{cat}) were calculated by dividing V_{max} with the concentration of the complex used.

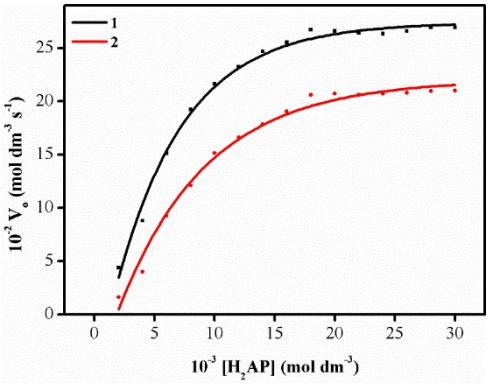

Fig. 7. Plot of initial rate vs. substrate concentration for the oxidation of H_2AP using 1 as catalyst in methanol

Table 3 - Kinetic parameters for phenoxazinone synthase activity of compounds **1** and **2**

Compound	V_{max} (mol dm^{-3} s^{-1})	K_M (mol dm^{-3})	kcat (h^{-1})
1	26.27 x 10^{-2}	5.11 x 10^{-3}	71.94
2	20.52 x 10^{-2}	6.52 x 10^{-3}	55.19

The turnover number (kcat) for **1** is higher than **2**, these results supports our observations from GC experiments.

To gain insights into the mechanistic aspects of the reaction, we then carried out ESI-MS of the reaction products of **1** and **2** by adding 5 eq. of H_2AP to solutions of **1** and **2**. ESI-MS showed the mass peak for the reduced species of copper(I) in addition to the mass peaks of **1** and **2**. In case of **1**, the peak at *m/z* 405.25 corresponds to $[Cu(BQEN)]^{1+}$ (calcd *m/z* 405.11) (Fig. S10) while for compound **2**, a new peak at *m/z* 419.25 correspond to $[Cu(BQPN)]^{1+}$ (calcd *m/z* 419.13) (Fig. 8). To further prove the existence of Cu(I) species in the end product, we also recorded the EPR spectrum of the end product mixture obtained after addition of the substrate of H_2PA to acetonitrile solution of **1** using spin-amount quantification of the EPR spectrum, it was found that the amount of Cu(II) during the reaction was reduced to 55 % in case of **1** (Fig. 9) and 52 % in case of **2** (Fig. S9) compared to that of the original spectra. The reduced area may be attributed to the reduction of Cu(II) to Cu(I). These results led us to propose a two-step mechanism for reaction of H_2AP with **1** and **2** (Scheme 2). In step (i) the H_2AP substrate binds to the Cu(II) centre by substituting a solvent molecule. The H_2AP is then deprotonated to form Cu(I)-(2- iminosemiquinonato) [Cu(I)-$(ISQ)^{\bullet-}$] radical anion. In successive stage the dioxygen then irreversibly oxidises radical anion to produce 2 electron oxidised product 2-benzoquinone monoamine (BQMI). In second step, the highly electrophilic BQMI then rapidly couple with second molecule of H_2AP in the presence of H_2O_2 resulting in the formation of desired product APX.

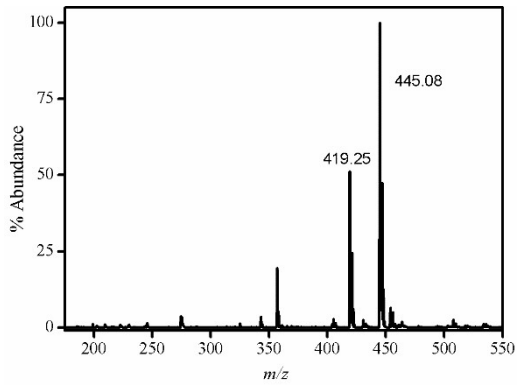

Fig. 8. ESI-MS of end metal product obtained after addition of 5 eq. H_2AP to the CH_3CN solution of **2**.

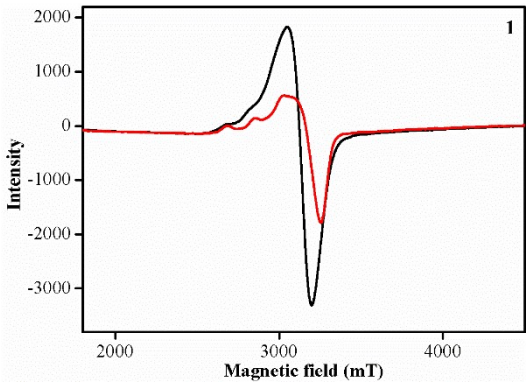

Fig. 9. X-band EPR spectra of **1** (black) and (red) after addition with 5 eq. H_2AP recorded at 77 K CH_3CN.

View Article Online
DOI: 10.1039/D2NJ04859K

The substrate can bind to the copper centre in monodentate as well as bidentate modes, however the bidentate mode will be preferred due to chelate effect. The binding of the substrate to the copper centre will be easier in **1** as it has square pyramidal geometry and the solvent molecule is easily displaced by an attack of the substrate from the vacant site. However, in case **2**, since its structure is intermediate between square planer and trigonal bipyramidal it will be difficult for the substrate to bind to the copper centre. Thus compound **2** has to undergo structural changes to accommodate the substrate at the active site. Whereas in case of **1** the reaction is SN^2 type where the substrate attacks from one side and the solvent molecule leaves from the other side. This also explains the lower TON of the product APX by **2** compared to the reaction of **1**.

In order to further gain the knowledge on the influence of steric factor on reactivity of **1** over **2**, we have performed computational studies and obtained their steric maps for **1** and **2**. The steric maps and percent buried volume (% Vbur) calculated for **1** and **2** are depicted in Fig. 10. The steric maps provide the information about the possible surface of interaction between the catalytically active metal atom and the substrate. The steric nature of the ligand possibly hinders substrate binding and leads to lower reactivity. The compounds with ligands having lower steric nature are known to show better catalytic activity and high TON [49]. The higher catalytic activity of **1** is thus attributed to its less steric nature (%Vbur, 71.3 %) as compared to that of **2** (%Vbur, 75.6 %) based on the steric map studies. Overall results suggest that increase in carbon number (en to pn) in the carbon chain backbone of ligand (BQPN) has not shown the distorted the geometry but also showed the effects on catalytic activity.

Conclusions

Mononuclear Cu(II) compounds **1** and **2** supported by quinoline based tetradentate nonheme ligands were synthesized and characterized. Both compounds have shown five coordination pentagonal geometries exhibiting interesting structural behaviours in terms of the degrees of distortions from a perfect square pyramid. Both compounds **1** and **2** showed good reactivity towards H_2AP and formed high yields of product APX thus exhibiting phenoxazinone synthase like activity. Higher TON numbers of APX in **1** are attributed to the lower steric effects of the BQEN ligand whereas lower TON in case **2** is attributed to the sterically hindered ligand BQPN. These results supported by the computational studies on steric maps which showed steric nature (%Vbur, 71.3 %) for **1** and (%Vbur, 75.6 %) for **2**.

Author contributions

SSH- Conceptualization**,** data curation**,** formal analysis**,** investigation, software, validation, writing and editing.
SND- Conceptualization, funding acquisition, Project administration, resources, supervision, writing – review & editing of the manuscript.
VRC – Computational studies and energy analysis.

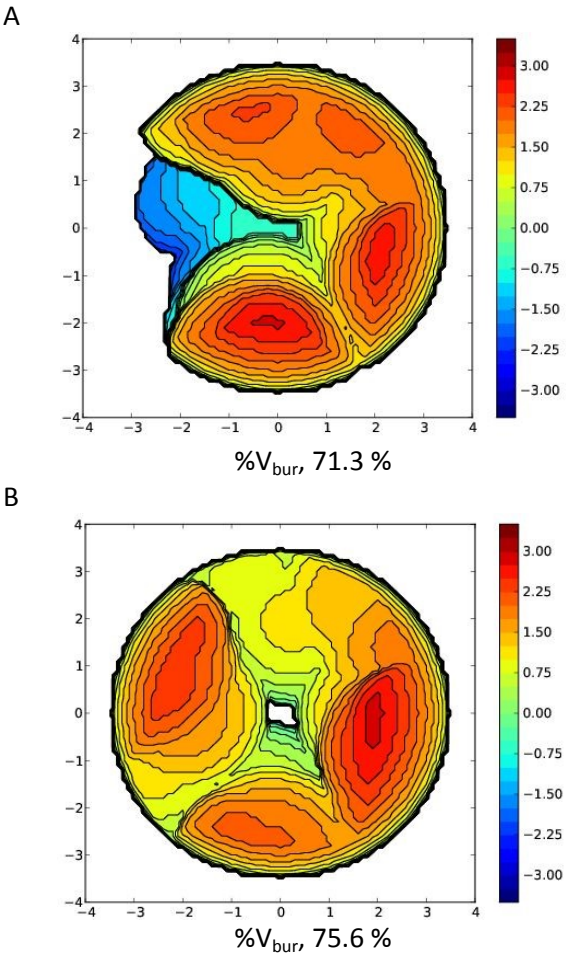

Fig. 10. Steric maps of compounds **a**) 1 and **b**) 2.

Conflicts of interest

There is no conflict of interest.

Acknowledgements

SND thank Council of Scientific and Industrial Research (CSIR), New Delhi, India (No. 01(2923)/18/EMR-II) for funding. SSH thanks UGC for NFOBC fellowship. Authors acknowledge DST fir funding of Single Crystal Diffractometer under DST-FIST program (SR/FST/CSII-034/2014).

References

1 (a) D. Bordo, D. Matak, K. Djinovic-Carugo, C. Rosano, A. Pesce, M. Bolognesi, M. E. Stroppolo, M. Falconi, A. Battistoni, A. Desideri, J. Mol. Biol., 1999, **285**, 283. (b) J. L. García-Giménez, G. Alzuet, M. González-Álvarez, M. Liu-González, A. Castiñeiras, J. Borrás, J. Mol. Biol., 2009, **103**, 243. (c) M. N. Isupov, A. R. Dalby, A. A. Brindley, Y. Izumi, T. Tanabe, G. N. Murshudov, J. A. Littlechild, J. Mol. Biol., 2000, **299**, 1035. (d) J-H. Li, J-T. Wang, Z-W. Mao, L.-N. Ji, Inorg. Chem. Commun., 2008, **11**, 865. (e) A. Myari, G. Malandrinos, Y. Deligiannakis, J. C. Plakatouras, N. Hadjiliadis, Z. Nagy, I. Sòvágó, J. Mol. Biol., 2001, **85**, 253. (f) G. Schenk, L. E. Carrington, M. Valizadeh J. de Jersey, S. E. Hamilton, L. W. Guddat, J. Mol. Biol., 2003, **96**, 225.

2 2 A. W. Addison, T. N. Rao, J. Reedijk, J. van Rijn, G. C. Verschoor, J. Chem, Soc, Dalton Trans., 1984, 1349.

3 3. L. Yang, D. R. Powell, R. P. Houser, Dalton Trans., 2007 955.

4 4. M. T. Miller, P. K. Gantzel, T. B. Karpishin, Inorg. Chem., 1998, 37 2285.

5 (a) V. Gandin, M. Porchia, F. Tisato, A. Zanella, E. Severin, A. Dolmella, C. Marzano, J. Med. Chem., 2013, 56, 7416; (b) A. Barve, A. Kumbhar, M. Bhat, B. Joshi, R. Butcher, U. Sonawane, R. Joshi, Inorg. Chem., 2009, 48, 9120; (c) R. Loganathan, S. Ramakrishnan, E. Suresh, A. Riyasdeen, M. A. Akbarsha, M. Palaniandavar, Inorg. Chem., 2012, 51, 5512; (d) S. Ramakrishnan, M. Palaniandavar, J. Chem. Sci., 2005, 117, 179; (e) X-Y. Qin, Y-N. Wang, X-P. Yang, J-J. Liang, J-L. Liua, Z-H. Luoa, Dalton Trans., 2017, 46, 16446; (f) S. Kathiresan, S. Mugesh, J. Annaraj, M. Muruganb, New J. Chem., 2017, 41, 1267; (g) W-J. Lian, X-T. Wang, C-Z. Xie, H. Tian, X-Q. Song, H-T. Pan, X. Qiao, J-Y. Xu, Dalton Trans., 2016, 45, 9073; (h) P. Jaividhya, M. Ganeshpandian, R. Dhivya, M. A. Akbarsha, M. Palaniandavar, Dalton Trans., 2015, 44, 11997.

6 K. A. Magnus, H. Ton-That, J. E. Carpenter, *Chem. Rev*., 1994, **94**, 727.

7 F. Fusetti, K. H. Schroter, R. A. Steiner, P. I. van Noort, T. Pijning, H. J. Rozeboom, K. H. Kalk, M. R. Egmond, B. W. Dijkstra, *Structure*, 2002, **10**, 259.

8 R. A. Steiner, I. M. Kooter, B. W. Dijkstra, *Biochem*, 2002, **41**, 7955.

9 I. M. Kooter, R. A. Steiner, B. W. Dijkstra, P. I. van Noort, M. R. Egmund, M. Huber, *Eur. J. Biochem*., 2002, **269**, 2971.

10 C. Gerdemann, C. Eicken, B. Krebs, *Acc. Chem. Res*., 2002, **35**, 183

11 A. Sa'nchez-Ferrer, J. N. Rodrı'guez-Lo'pez, V. Garcı'a-Ca'novas, F.G. Carmona, *Biochim. Biophys. Acta*, 1995, **1**, 1247.

12 H. -H. T. Nguyen, K. H. Nakagawa, B. Hedman, S. J. Eliot, M. E. Lidstrom, K. O. Hodgson, S. I. Chan, *J. Am. Chem. Soc*., 1996, **118**, 12766.

13 S. J. Elliott, D. W. Randall, R. D. Britt, S. I. Chan, *J. Am. Chem. Soc*., 1998, **120**, 3247.

14 R. L. Lieberman, D. B. Shrestha, P. E. Doan, B. M. Hoffman, T. L. Stemmler, A. C. Rosenzweig, *Proc. Natl. Acad. Sci. Unit. States Am*., 2003, **100**, 3820.

15 J. W. Whittaker, *Chem. Rev*., 2003, **103**, 2347.

16 M. Halcrow, S. Phillips, P. Knowles, in: A. Holzenburg, N.S. Scrutton (Eds.), Subcellular Biochemistry, Enzyme-Catalyzed Electron and Radical Transfer, Plenum, New York, 2000, 183.

17 M. M. Whittaker, P. J. Kersten, N. Nakamura, J. Sanders-Loehr, E. S. Schweizer, J. W. Whittaker, *J. Biol. Chem*., 1996, **271**, 681.

18 M. M. Whittaker, P. J. Kersten, D. Cullen and J. W. Whittaker, *J. Biol. Chem*., 1999, **274**, 36226.

19 C. E., III Barry, P. G. Nayar and T. P. Begley, *J. Am. Chem. Soc*., 1988, **110**, 3333.

20 C. E., III Barry, P. G. Nayar and T. P. Begley, *Biochemistry*, 1989, **28**, 6323.

21 J. C. Freeman, P. G. Nayar, T. P. Begley and J. J. Willafranca, Biochemistry, 1993, **32**, 4826.

22 A. W. Smith, A. Camara-Artigas, M. Wang, J. P. Allen and W. A. Francisco, *Biochemistry*, 2006, **45**, 4378.

23 S. K. Dey and A. Mukherjee, *Coord. Chem. Rev*., 2016, **310**, 80.

24 E. Katz, in: D. Gottlieb, P.D. Shaw (Eds.), Biosynthesis of Secondary Metabolites: Roles of Trace Metals Antibiotics II, Springer, New York, 1967, 276.

25 U. Hollstein, *Chem. Rev*., 1974, **74**, 625.

26 (a) A. Butenandt, *Angew. Chem*., 1957, **69**, 16; (b) T. M. Simándi, L. I. Simándi, M. Györ, A. Rockenbauer and A. Gömöry, *J. Chem. Soc. Dalton Trans*., 2004, 1056.

27 (a) G. W. K. Cavill, P. S. Clezy, J. R. Tetaz and R. L. Werner, *Tetrahedron*, 1959, **5**, 275; (b) J. Kaizer, R. Csonka and G. Speier, *J. Mol. Catal. A: Chem*., 2002, **180**, 91.

28 C. Mukherjee, T. Weyhermuller, E. Bothe, E. Rentschler and P. Chaudhuri, *Inorg. Chem*., 2007, **46**, 9895.

29 (a) M. Mitra, T. Kundu, G. Kaur, G. Sharma, A. R. Choudhury, Y. Singh and R. Ghosh, *RSC Adv*., 2016, **6**, 58831; (b) S. Sagar, S. Sengupta, A. J. Mota, S. K. Chattopadhyay, A. E. Ferao, E. Riviere, W. Lewis and S. Naskar, *Dalton Trans*., 2017, **46**, 1249; (c) O. V. Nesterova, O. E. Bondarenko, A. J. L. Pombeiro and D. S. Nesterov, *Dalton Trans*., 2020, **49**, 4710.

30 (a) P. Mahapatra, S. Ghosh, S. Giri, V. Rane, R. Kadam, M. G. B. Drew and A. Ghosh, *Inorg. Chem*., 2017, **56**, 5105. (b) P. Mahapatra, M. G. B. Drew and A. Ghosh, *Cryst. Growth Des*., 2017, **17**, 6809; (c) S. Dutta, J. Mayans and A. Ghosh, *Dalton Trans*., 2020, **49**, 1276.

31 (a) A. K. Ghosh, A. Ali, Y. Singh, C. S. Purohit and R. Ghosh, *Inorg. Chim. Acta*., 2018, **474**, 156; (b) D. Mondal, A. K. Ghosh, A. Chatterjee and R. Ghosh, *Inorg. Chim. Acta*., 2019, **486**, 719; (c) T. Dutta, S. Mirdya, P. Giri and S. Chattopadhyay, *Polyhedron*, 2020, **175**, 114164; (d) S. Roy, T. Dutta, M. G. B. Drew and S. Chattopadhyay, *Polyhedron*, 2020, **178**, 114311; (e) P. K. Mudi, N. Bandopadhyay, M. Joshi, M. Shit, S. Paul, A. R. Choudhury and B. Biswas, *Inorg. Chim. Acta*., 2020, **505**, 119468.

32 (a) T. Horvath, J. Kaizer and G. Speier, *J. Mol. Catal. A: Chem*., 2004, **215**, 9; (b) M. R. Maurya, S. Sikarwar, T. Joseph and S.B. Halligudi, *J. Mol. Catal. A: Chem*., 2005, **236**, 132; (c) B. Chowdhury, M. Maji and B. Biswas, *J. Chem. Sci*., 2017, **129**, 1627; (d) W. P. Sohtun, S. Muthuramalingam, M. Velusamy and R. Mayilmurugan, *Inorg. Chem. Comm*., 2019, **110**, 107608; (e) A. E.-M. M. Ramadan, S. Y. Shaban, M. M. Ibrahim, A. A.-H. Abdel-Rahman, S. A. Sallam, S. A. Al- Harbi and W. Omar, *New J. Chem*., 2020, **44**, 6331.

33 (a) I. C. Szigyarto, T. M. Simandi, L. I. Simandi, L. Korecz and N. Nagy, *J. Mol. Catal. A: Chem*., 2006, **251**, 270; (b) C. Mukherjee, T. Weyhermuller, E. Bothe and P. Chaudhuri, *C. R. Chimie*, 2007, **10**, 313; (c) J. Kaizer, G. Barath, R. Csonka, G. Speier, L. Korecz, A. Rockenbauer and L. Parkanyi, *J. Inorg. Biochem*., 2008, **102**, 773; (d) A. Panja, *Polyhedron*, 2014, **79**, 258; (e) A. Panja, *RSC Adv*., 2014, **4**, 37085; (f) S. C. Kumar, A. K. Ghosh, J-D. Chen and R. Ghosh, *Inorg. Chim. Acta*., 2017, **464**, 49.

34 M. Ismael, AM. M. Abdel-Mawgoud, M. K. Rabia and A. Abdou, *Inorg. Chim. Acta*., 2020, **505**, 119443.

35 (a) L. I. Simandi, T. Barna and S. Nemeth, *J. Chem. Soc., Dalton Trans*., 1996, 473; (b) A. Panja, M. Shyamal, A. Saha and T. K. Mandal, *Dalton Trans*., 2014, **43**, 5443; (c) A. Panja, *Dalton*

View Article Online
DOI: 10.1039/D2NJ04859K

Trans., 2014, **43**, 7760 (d) M. Mahato, D. Mondal and H. P. Nayek, *ChemistrySelect*, 2016, **2**, 67772; (e) K. Ghosh, K. Harms and S. Chattopadhyay, *ChemistrySelect*, 2017, **2**, 8207; (f) N. C. Jana, M. Patra, P. Brandao and A. Panja, *Polyhedron*, 2019, **164**, 23.

36 (a) D. D. Narulkar, A. R. Patil, C. C. Naik and S. N. Dhuri, *Inorg. Chim. Acta*, 2015, **427**, 248 (b) D.D. Narulkar, A. K. Srivastav, R. J. Butcher, K. M. Ansy, S. N. Dhuri, *Inorg. Chim. Acta*, 2017, **467**, 405-414.

37 G. M. Sheldrick, *Acta Crystallogr*., 2015, **C71**, 3-8.

38 Gaussian 16, Revision C.01, M. J. Frisch, G. W. Trucks, H. B. Schlegel, G. E. Scuseria, M. A. Robb, J. R. Cheeseman, G. Scalmani, V. Barone, G. A. Petersson, H. Nakatsuji, X. Li, M. Caricato, A. V. Marenich, J. Bloino, B. G. Janesko, R. Gomperts, B. Mennucci, H. P. Hratchian, J. V. Ortiz, A. F. Izmaylov, J. L. Sonnenberg, D. Williams-Young, F. Ding, F. Lipparini, F. Egidi, J. Goings, B. Peng, A. Petrone, T. Henderson, D. Ranasinghe, V. G. Zakrzewski, J. Gao, N. Rega, G. Zheng, W. Liang, M. Hada, M. Ehara, K. Toyota, R. Fukuda, J. Hasegawa, M. Ishida, T. Nakajima, Y. Honda, O. Kitao, H. Nakai, T. Vreven, K. Throssell, J. A. Montgomery, Jr., J. E. Peralta, F. Ogliaro, M. J. Bearpark, J. J. Heyd, E. N. Brothers, K. N. Kudin, V. N. Staroverov, T. A. Keith, R. Kobayashi, J. Normand, K. Raghavachari, A. P. Rendell, J. C. Burant, S. S. Iyengar, J. Tomasi, M. Cossi, J. M. Millam, M. Klene, C. Adamo, R. Cammi, J. W. Ochterski, R. L. Martin, K. Morokuma, O. Farkas, J. B. Foresman, and D. J. Fox Gaussian, Inc., Wallingford CT, 2016.

39 A. Poater, B. Cosenza, A. Correa, S. Giudice, F. Ragone, V. Scarano, L. Cavallo, Chem. Eur. J., 2010, **16**, 14348.

40 B. J. Pella, J. Niklas, O. G. Poluektov, A. Mukherjee, *Inorg. Chim. Acta*, 2018, **483**, 71. (b) N. Singh, J. Niklas, O. G. Poluektov, K. M. Van Heuvelen, A. Mukherjee, *Inorg. Chim. Acta*, 2017, **455**, 221. (c) R. L. Chapman, F. S. Stephens, R. S. Vagg, *Inor. Chim. Acta*, 1980, **43**, 29.

41 E. Garribba, G. Micera, J. Chem. Educ., 2006, 83, 1229.

42 (a)T. Lu, X. Zhuang, Y. Li and S. Chen, J. Am. Chem. Soc., 2004, **126**, 4760–4761. (b)A. Grirrane, E. Álvarez, J. Albero, H. García and A. Corma, Dalton Trans., 2016, **45**, 5444–5450.

43 K. Nakamoto, Infrared Spectra and Raman Spectra of Inorganic and Coordination Compound Part B: Application in Coordination, Organometallic and Bioinorganic Chemistry, 6th Ed., (John Wiley, Hoboken, NJ) (2009) 88.

44 S. Thakurta, J. Chakraborty, G. Rosair, J. Tercero, M. S. El Fallah, E. Garribba and S. Mitra, *Inorg. Chem.*, 2008, **47**, 6227.

45 J. R. Hartman, R. W. Vachet, W. Pearson, R. J. Wheat, J. H. Callahan, *Inorg. Chim. Acta*, 2003, **343**, 119.

46 S. S. Harmalkar, R. J. Butcher, V. V. Gobre, S. K. Gaonkar, L. R. D'Souza, M. Sankaralingam, I. Furtado, S. N. Dhuri, *Inorg. Chim. Acta*, 2019, **498**, 1190202.

47 (a) E. Katz 1967 Biosynthesis of secondary metabolites: roles of trace metals In Antibiotics II D. Gottlieb and P. D. Shaw (Eds.) p. 276 (New York: Springer); (b) J. McLain, J. Lee, J. T. Groves, 2000 Biomimetic oxidations catalyzed by transition metal complexes In Biomimetic Oxidations Catalyzed by Transition Metal Complexes B Meunier (Ed.) (London: Imperial College Press)

48 J. H. Espenson, *Chem. Kinet. React. Mech.*, McGraw-Hill, 1995, 70-100.

49 W. P. Sohtun, S. Muthuramalingam, M. Sankaralingam, M. Velusamy, R.Mayilmurugan, *J. Inorg. Biochem*., 2021, **216,** 111313.